Research Article | Vol. 25, No. 13 | 26 Jun 2017 | OPTICS EXPRESS 14049
Optics EXPRESS

Aberrations in 4Pi Microscopy

XIANG HAO,[1] JACOPO ANTONELLO,[2] EDWARD S. ALLGEYER,[3] JOERG BEWERSDORF,[1,4,6] AND MARTIN J. BOOTH[2,5,7]

[1]*Department of Cell Biology, Yale School of Medicine, New Haven, Connecticut 06520, USA*
[2]*Centre for Neural Circuits and Behaviour, University of Oxford, Oxford OX1 3SR, UK*
[3]*The Gurdon Institute, University of Cambridge, Cambridge CB2 1QN, UK*
[4]*Department of Biomedical Engineering, Yale University, New Haven, Connecticut 06510, USA*
[5]*Department of Engineering Science, University of Oxford, Oxford OX1 3PJ, UK*
[6]*joerg.bewersdorf@yale.edu*
[7]*martin.booth@eng.ox.ac.uk*

Abstract: The combination of two opposing objective lenses in 4Pi fluorescence microscopy significantly improves the axial resolution and increases the collection efficiency. Combining 4Pi microscopy with other super-resolution techniques has resulted in the highest three-dimensional (3D) resolution in fluorescence microscopy to date. It has previously been shown that the performance of 4Pi microscopy is significantly affected by aberrations. However, a comprehensive description of 4Pi microscope aberrations has been missing. In this paper, we introduce an approach to describe aberrations in a 4Pi cavity through a new functional representation. We discuss the focusing properties of 4Pi systems affected by aberrations and discuss the implications for adaptive optics schemes for 4Pi microscopes based on this new insight.

OCIS codes: (180.6900) Three-dimensional microscopy; (220.1010) Aberrations (global); (220.1080) Active or adaptive optics.

References and links

1. S. W. Hell, "Double-confocal scanning microscope," Euro Patent EP0491289 B1 (1996).
2. H. Gugel, J. Bewersdorf, S. Jakobs, J. Engelhardt, R. Storz, and S. W. Hell, "Cooperative 4Pi excitation and detection yields sevenfold sharper optical sections in live-cell microscopy," Biophys. J. **87**(6), 4146–4152 (2004).
3. J. Bewersdorf, R. Schmidt, and S. W. Hell, "Comparison of I^{5}M and 4Pi-microscopy," J. Microsc. **222**(2), 105–117 (2006).
4. M. G. L. Gustafsson, L. Shao, P. M. Carlton, C. J. R. Wang, I. N. Golubovskaya, W. Z. Cande, D. A. Agard, and J. W. Sedat, "Three-dimensional resolution doubling in wide-field fluorescence microscopy by structured illumination," Biophys. J. **94**(12), 4957–4970 (2008).
5. S. W. Hell, S. Lindek, C. Cremer, and E. H. K. Stelzer, "Measurement of the 4Pi-confocal point spread function proves 75 nm axial resolution," Appl. Phys. Lett. **64**(11), 1335–1337 (1994).
6. R. Schmidt, C. A. Wurm, S. Jakobs, J. Engelhardt, A. Egner, and S. W. Hell, "Spherical nanosized focal spot unravels the interior of cells," Nat. Methods **5**(6), 539–544 (2008).
7. M. Dyba and S. W. Hell, "Focal spots of size λ/23 open up far-field fluorescence microscopy at 33 nm axial resolution," Phys. Rev. Lett. **88**(16), 163901 (2002).
8. G. Shtengel, J. A. Galbraith, C. G. Galbraith, J. Lippincott-Schwartz, J. M. Gillette, S. Manley, R. Sougrat, C. M. Waterman, P. Kanchanawong, M. W. Davidson, R. D. Fetter, and H. F. Hess, "Interferometric fluorescent super-resolution microscopy resolves 3D cellular ultrastructure," Proc. Natl. Acad. Sci. U.S.A. **106**(9), 3125–3130 (2009).
9. D. Aquino, A. Schönle, C. Geisler, C. V. Middendorff, C. A. Wurm, Y. Okamura, T. Lang, S. W. Hell, and A. Egner, "Two-color nanoscopy of three-dimensional volumes by 4Pi detection of stochastically switched fluorophores," Nat. Methods **8**(4), 353–359 (2011).
10. F. Huang, G. Sirinakis, E. S. Allgeyer, L. K. Schroeder, W. C. Duim, E. B. Kromann, T. Phan, F. E. Rivera-Molina, J. R. Myers, I. Irnov, M. Lessard, Y. Zhang, M. A. Handel, C. Jacobs-Wagner, C. P. Lusk, J. E. Rothman, D. Toomre, M. J. Booth, and J. Bewersdorf, "Ultra-high resolution 3D imaging of whole cells," Cell **166**, 1–13 (2016).
11. U. Böhm, S. W. Hell, and R. Schmidt, "4Pi-RESOLFT nanoscopy," Nat. Commun. **7**, 10504 (2016).
12. X. Hao, E. S. Allgeyer, M. J. Booth, and J. Bewersdorf, "Point-spread function optimization in isoSTED nanoscopy," Opt. Lett. **40**(15), 3627–3630 (2015).

#296111 https://doi.org/10.1364/OE.25.014050
Journal © 2017 Received 18 May 2017; accepted 24 May 2017; published 12 Jun 2017

Optics EXPRESS

13. F. Zernike, "Beugungstheorie des Schneidenverfahrens und seiner verbesserten Form, der Phasenkontrastmethode," Physica **1**(7-12), 689–704 (1934).
14. M. Born and E. Wolf, *Principles of Optics* (Cambridge University Press, 1999).
15. S. W. Hell, R. Schmidt, and A. Egner, "Diffraction-unlimited three-dimensional optical nanoscopy with opposing lenses," Nat. Photonics **3**(7), 381–387 (2009).
16. R. J. Noll, "Zernike polynomials and atmospheric turbulence," J. Opt. Soc. Am. **66**(3), 207–211 (1976).
17. B. Richards and E. Wolf, "Electromagnetic diffraction in optical systems II. Structure of the image field in an aplanatic system," P. Roy. Soc. A-Math. Phys. **253**, 358–379 (1959).
18. X. Hao, C. Kuang, T. Wang, and X. Liu, "Effects of polarization on the de-excitation dark focal spot in STED microscopy," J. Opt. **12**(11), 115707 (2010).
19. K. Bahlmann and S. W. Hell, "Polarization effects in 4Pi confocal microscopy studied with water-immersion lenses," Appl. Opt. **39**(10), 1652–1658 (2000).
20. F. Curdt, S. J. Herr, T. Lutz, R. Schmidt, J. Engelhardt, S. J. Sahl, and S. W. Hell, "isoSTED nanoscopy with intrinsic beam alignment," Opt. Express **23**(24), 30891–30903 (2015).
21. M. J. Booth, "Adaptive optical microscopy: the ongoing quest for a perfect image," Light Sci. Appl. **3**(4), e165 (2014).
22. S. Liu, E. B. Kromann, W. D. Krueger, J. Bewersdorf, and K. A. Lidke, "Three dimensional single molecule localization using a phase retrieved pupil function," Opt. Express **21**(24), 29462–29487 (2013).
23. E. B. Kromann, T. J. Gould, M. F. Juette, J. E. Wilhjelm, and J. Bewersdorf, "Quantitative pupil analysis in stimulated emission depletion microscopy using phase retrieval," Opt. Lett. **37**(11), 1805–1807 (2012).

1. Introduction

The resolution of fluorescence microscopy is largely determined by the extent of the point-spread function (PSF). In single-objective imaging systems, the PSF is typically characterized by its prolate spheroidal shape: the axial (z) resolution of a microscope is always worse than the lateral (xy) resolution. This fundamental limit has made isotropic imaging of 3D structures difficult. To compress the PSF axially, 4Pi microscopy and related techniques such as I5M were developed [1–4]. In 4Pi microscopy, the laser beam in a confocal laser scanning microscope is divided into two arms (the 'upper' and 'lower' arms) that are focused by two opposing objectives into a common spot, creating an interferometric cavity. This additional interference around the focal region significantly sharpens the PSF along the optical axis, improving the axial resolution 3 to 7-fold [5]. In conjunction with super-resolution imaging methods, such as stimulated emission depletion nanoscopy (STED-4Pi or isoSTED) [6,7], single-molecule switching nanoscopy (4Pi-SMS or iPALM) [8–10], or reversible saturable optical fluorescence transition nanoscopy (4Pi-RESOLFT) [11], 4Pi microscopes have been the most efficient way to improve the axial resolution, and are able to reach 10 to 40 nm resolution in all three dimensions, providing multi-color, 3D, whole-cell images for biological applications.

As with all microscopes, aberrations introduced by the optical system or the specimen affect the focusing properties of a 4Pi microscope. In most cases, this leads to decreased imaging performance. Introducing specific aberrations can, however, also improve some desirable properties of the PSF [12]. Importantly, 4Pi microscopes react to aberrations quite differently from single-objective systems. Having the tools to describe 4Pi aberrations and understand how they affect the shape of the focal intensity, and hence the PSF, is therefore a prerequisite to fully optimize 4Pi microscope PSFs and to comprehend, and possibly counteract, the influence of specimens with heterogeneous refractive index.

In this paper, we provide a strategy for understanding aberration effects in 4Pi microscopy. We introduce a set of basis functions based on Zernike polynomials [13, 14] that express practically relevant physical phenomena such as interference fringe shifts, focal displacements, and distortions such as astigmatism, coma and spherical aberrations. Using this new basis, we examine their effects on the 4Pi focal intensity in a polarization-independent and dependent manner. This provides insight into the control of adaptive optical systems for aberration correction in 4Pi microscopes.

Optics EXPRESS

2. Aberration model for 4Pi microscopy

A 4Pi microscope can naively be considered as two separate microscopes: an upper and a lower microscope, configured to operate in conjunction with each other. This approach neglects, however, that the beams traveling the upper and lower beam paths of the 4Pi microscope interfere in the common focus. For example, in single-objective imaging systems, piston, the first Zernike polynomial, is usually irrelevant, since it does not cause deformations of the wavefront and therefore does not impact the measured PSF (Fig. 1(a)). However, in 4Pi microscopes, different piston combinations are associated with the phase shift of the interfering counter-propagating waves of the 4Pi-cavity and lead to significantly different focal intensities. (Figs. 1(b) and 1(c)).

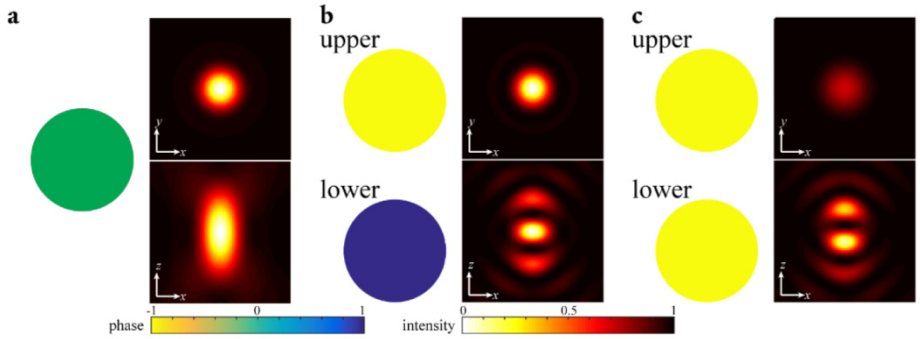

Fig. 1. Focal intensities with piston modes in (a) a single-objective microscope and (b~c) a 4Pi microscope. For the 4Pi microscope, the interference fringes are shifted along the optical axis when different pistons are applied to the two arms (upper and lower) in the 4Pi-cavity. Results in (b) and (c) are calculated for a mode coefficient value of 1 rad (~0.16 λ) rms.

A better approach is to consider the whole 4Pi microscope as a single optical system with an extended pupil consisting of two non-contiguous circular pupils representing the two objectives [15]. To describe aberrations in such a system, we need a set of orthogonal basis functions that is complete, i.e. capable of describing arbitrary (sufficiently smooth) aberrations. Individual basis functions should ideally represent practically relevant phenomena, such as focal shifts or typical aberration modes that commonly arise in microscopes. As an analogy, in single-objective systems, the Zernike polynomials are convenient as the lower order modes tip, tilt and defocus correspond to focal shifts in three dimensions, whereas higher order modes relate to coma, astigmatism, spherical aberration and so on.

To carry out this analysis, we need to define the relationship between coordinates for the upper and lower pupils, P_u and P_l. These pupils are conceived in the well-established manner of mapping the spherical cap-shaped input pupil of the objective onto the circular output pupil by means of the sine condition. We introduce a new coordinate system composed of two independent sets of Cartesian coordinates, $\left(x_u, y_u, z_u\right)$ and $\left(x_l, y_l, z_l\right)$, corresponding to the upper and lower beam paths, respectively (Fig. 2). The relative orientation of the unit vectors is defined by the optical imaging properties through the objective pair, which mirrors the coordinate system along the x and y axes, but not the z axis. This arrangement helps maintain an optically conjugated relationship between the pupils, while the orientation of the z unit vector in both coordinate systems represents the propagation direction of a beam approaching the objective pair from the upper beam path. The relationship between these two coordinate systems is expressed as:

Optics EXPRESS

$$\begin{aligned}\hat{\mathbf{x}}_u &= -\hat{\mathbf{x}}_l \\ \hat{\mathbf{y}}_u &= -\hat{\mathbf{y}}_l \\ \hat{\mathbf{z}}_u &= \hat{\mathbf{z}}_l\end{aligned} \tag{1}$$

where $\hat{\mathbf{x}}$, $\hat{\mathbf{y}}$, and $\hat{\mathbf{z}}$ are unit vectors along the corresponding axes. As a result, an aberration mode describing a positive phase delay in the lower pupil for a beam coming in from the lower beam path has opposite sign to a beam coming in from the upper beam path in the upper pupil. Furthermore, a ray entering the upper pupil at position (ζ,η) will exit the lower pupil at (ζ,η). As we will show below, an advantage of this arrangement is that when the incident beams are unpolarized, the shape of the focal intensity induced by aberrations in the upper pupil would be identical to that of focal intensity from the lower pupil when the same aberration function is applied.

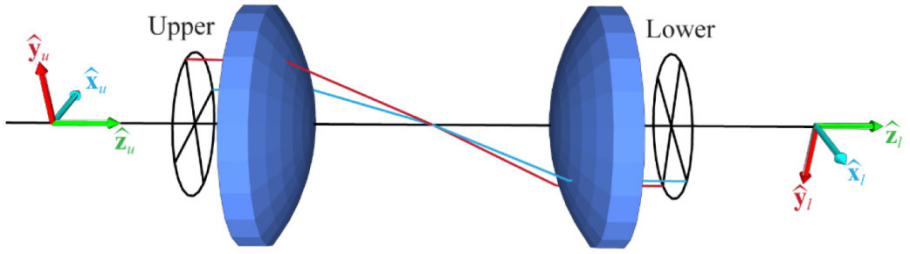

Fig. 2. The coordinate system for the 4Pi aberration modes.

Based on the coordinate system defined above, we take two identical sets of Zernike polynomials $\{Z_i(\mathbf{r})\}$ defined in the upper and lower pupils, P_u and P_l, respectively. Without loss of generality, we assume normalized coordinates such that both pupils are unit circles. We follow Noll's definition of Zernike polynomials with i being the Noll index [16], where i is a single index used as a convenient alternative to the common radial and azimuthal indices. Based on these two sets, we form a new basis set of 4Pi modes $\{Q_i^s(\mathbf{r})\}$:

$$Q_i^s(\mathbf{r}) = \begin{cases} Z_i(\mathbf{r}) & \text{for } \mathbf{r} \in P^u \\ s \cdot Z_i(\mathbf{r}) & \text{for } \mathbf{r} \in P^l \end{cases} \tag{2}$$

where $s = \pm 1$ represents whether the two pupils are in phase or anti-phase. $\{Q_i^{+1}(\mathbf{r})\}$ corresponds to "covariant" modes, where the same single-objective focal intensity is created by each path when seen separately. $\{Q_i^{-1}(\mathbf{r})\}$ in contrast corresponds to "contra-variant" modes where the two objectives create opposite effects (anti-phase). Following this recipe *ad infinitum* provides a complete set of orthogonal 4Pi modes as proven below.

We define the inner product of two 4Pi modes as:

Optics EXPRESS

$$\begin{aligned}\left\langle Q_i^s, Q_{i'}^{s'}\right\rangle &= \frac{1}{A}\int_{P_u\cup P_l} Q_i^s(\mathbf{r}) Q_{i'}^{s'}(\mathbf{r})\, d^2\mathbf{r} \\ &= \frac{1}{2\pi}\int_{P_u} Z_i(\mathbf{r}) Z_{i'}(\mathbf{r})\, d^2\mathbf{r} + \frac{1}{2\pi}\int_{P_l} s\cdot s' Z_i(\mathbf{r}) Z_{i'}(\mathbf{r})\, d^2\mathbf{r} \\ &= \frac{(1+ss')}{2\pi}\int_0^1\int_0^{2\pi} Z_i(\varphi,l)\cdot Z_{i'}(\varphi,l)\cdot l\, dl\, d\varphi \\ &= \delta_{s,s'}\left\langle Z_i, Z_{i'}\right\rangle_1\end{aligned} \tag{3}$$

where A represents the area of the combined pupil $P_u \cup P_l$, which has value 2π. φ and l are respectively the azimuthal angle and radius of a point inside the pupil. The expression $\left\langle Z_i, Z_{i'}\right\rangle_1$ represents the usual inner product between Zernike polynomials. Since Zernike polynomials are orthogonal for circular pupils, the orthogonality of the 4Pi modes is confirmed by Eq. (3).

Similarly, we prove that the new set of 4Pi modes is complete. Any sufficiently smooth real-valued phase function $\Phi(\mathbf{r}) \in \mathcal{L}^2$ defined in the two pupils can be split into two phase functions defined in the upper and lower pupil, respectively. These phase functions in turn can be expressed as linear combinations of Zernike modes, which form a complete basis in each individual objective pupil:

$$\Phi(\mathbf{r}) = \begin{cases}\Phi_u(\mathbf{r}) \text{ for } \mathbf{r}\in P_u \\ \Phi_l(\mathbf{r}) \text{ for } \mathbf{r}\in P_l\end{cases} = \begin{cases}\sum_{i=1}^{\infty} a_i\cdot Z_i(\mathbf{r}) \text{ for } \mathbf{r}\in P_u \\ \sum_{i=1}^{\infty} b_i\cdot Z_i(\mathbf{r}) \text{ for } \mathbf{r}\in P_l\end{cases} \tag{4}$$

We further define two sets of new basis functions as follow:

$$R_i^+(\mathbf{r}) = \frac{1}{2}\left[Q_i^{+1}(\mathbf{r}) + Q_i^{-1}(\mathbf{r})\right] = \begin{cases}Z_i(\mathbf{r}) & \text{for } \mathbf{r}\in P_u \\ 0 & \text{for } \mathbf{r}\in P_l\end{cases} \tag{5}$$

$$R_i^-(\mathbf{r}) = \frac{1}{2}\left[Q_i^{+1}(\mathbf{r}) - Q_i^{-1}(\mathbf{r})\right] = \begin{cases}0 & \text{for } \mathbf{r}\in P_u \\ Z_i(\mathbf{r}) & \text{for } \mathbf{r}\in P_l\end{cases} \tag{6}$$

Substituting Eqs. (5) and (6) into Eq. (4), we can write:

$$\begin{aligned}\Phi(\mathbf{r}) &= \sum_{i=1}^{\infty} a_i\cdot R_i^+(\mathbf{r}) + \sum_{i=1}^{\infty} b_i\cdot R_i^-(\mathbf{r}) \\ &= \sum_{i=1}^{\infty}\frac{1}{2}a_i\cdot\left[Q_i^{+1}(\mathbf{r}) + Q_i^{-1}(\mathbf{r})\right] + \sum_{i=1}^{\infty}\frac{1}{2}b_i\cdot\left[Q_i^{+1}(\mathbf{r}) - Q_i^{-1}(\mathbf{r})\right] \\ &= \sum_{i=1}^{\infty} c_i Q_i^{+1}(\mathbf{r}) + d_i Q_i^{-1}(\mathbf{r})\end{aligned} \tag{7}$$

where $c_i = \frac{1}{2}a_i + \frac{1}{2}b_i$ and $d_i = \frac{1}{2}a_i - \frac{1}{2}b_i$. Hence, any phase function $\Phi(\mathbf{r})$ can be expressed as a linear combination of 4Pi modes $\left\{Q_i^s(\mathbf{r})\right\}$ and is therefore complete. It is interesting to note that the approach we present here for forming any aberration in 4Pi microscopy based on the Zernike functions, is also valid for any other basis that is complete and orthogonal on a single pupil.

Optics EXPRESS

The first 24 4Pi aberration modes are shown in Fig. 3. Their distortion effects on the focal intensity are calculated using the vectorial theory described by Richards and Wolf [17,18]. We assume a 4Pi microscope with two identical objectives with a numerical aperture (NA) of 1.35 focusing into a medium of refractive index 1.406 and unpolarized input beams of equal intensity and uniform intensity distributions. When the input beams are unpolarized, we can calculate the focal intensity as:

$$I_{un} = \frac{1}{2}\left(I_x + I_y\right) \tag{8}$$

where I_x and I_y are the focal intensities when the input beams are x and y-polarized, respectively.

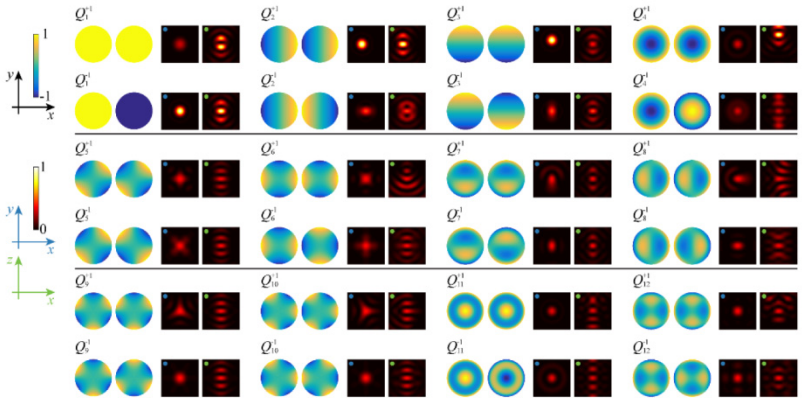

Fig. 3. 4Pi aberration modes. For each mode, the two pupil phase functions as well as $xy\,|_{z=0}$ (blue dot) and $xz\,|_{y=0}$ (green dot) cross-sections through the resulting 4Pi-PSF are shown. All results are calculated for a mode coefficient value of 1 rad (~0.16 λ). All focal intensities are normalized to the maximum of the aberration-free focal intensity (equivalent to that shown for Q_1^{-1}).

3. Discussion

Based on the above results, we can classify the new 4Pi modes in a manner similar to the arrangement of Zernike polynomials:

- Piston mode (mode Q_1^{-1}) – This mode has no effect on the intensity distribution. It is generated by the contra-variant combination of Zernike piston in the upper and lower paths.
- Fringe-shift mode (mode Q_1^{+1}) – This mode is the covariant combination of piston in the upper and lower paths that shifts the interference fringes along the optical axis.
- Displacement modes, which only translate the focus but do not change its shape, i.e. tip, tilt and defocus (modes Q_2^{+1}, Q_3^{+1} and Q_4^{+1}) – The covariant combinations of the respective Zernike modes in the upper and lower paths.
- Anti-displacement modes (modes Q_2^{-1}, Q_3^{-1}, and Q_4^{-1}) – The contra-variant combinations of tip, tilt and defocus Zernike modes. Phenomenologically, drift of one of the two objectives with respect to the other in the x, y or z-direction leads to the same focal intensity distortions.

Optics EXPRESS

Higher order modes can similarly be separated into covariant (e.g. 4Pi coma mode Q_7^{+1} and 4Pi spherical aberration mode Q_{11}^{+1}) and contra-variant modes (e.g. 4Pi anti-coma mode Q_7^{-1} and 4Pi anti-spherical aberration mode Q_{11}^{-1}). The focal intensities corresponding to covariant 4Pi modes can be interpreted as being similar to the focal intensities for the respective Zernike modes in a single-objective system, but modulated by the standing wave pattern resulting from the geometrical arrangement of the two opposing objectives (Figs. 4(a) and 4(c)).

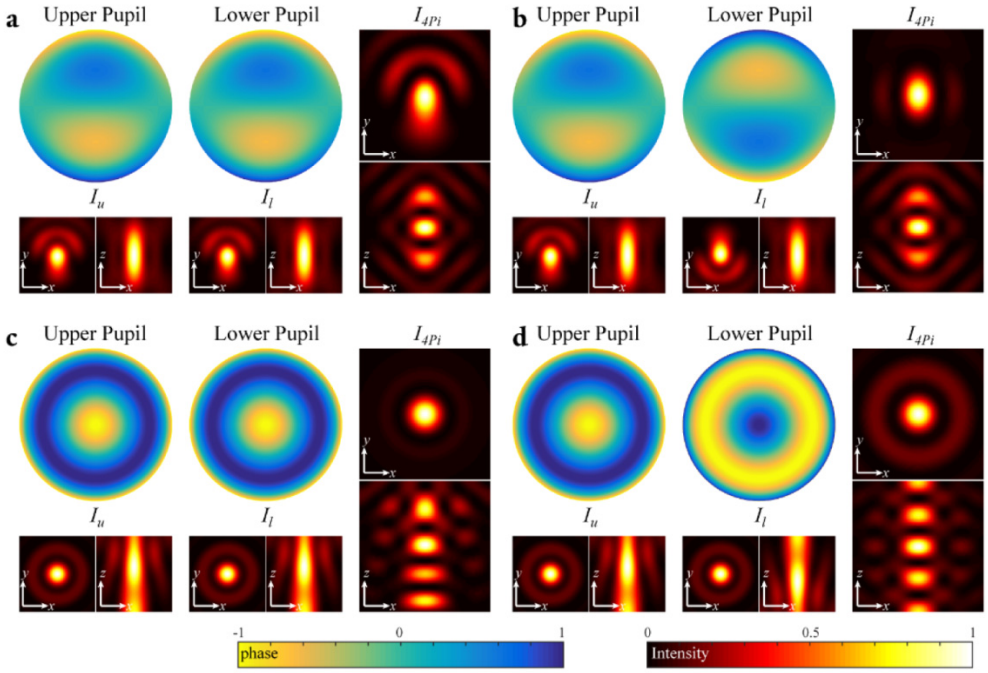

Fig. 4. Comparison of covariant (a, c) and contra-variant (b, d) 4Pi aberration modes. (a) shows the upper and lower pupil functions of 4Pi coma mode (Q_7^{+1}) and its effect on the focal intensity distribution, while (b-d) are for anti-coma (Q_7^{-1}), spherical aberration (Q_{11}^{+1}), and anti-spherical aberration modes (Q_{11}^{-1}), respectively. Underneath each pupil phase function, the $xy|_{z=0}$ and $xz|_{y=0}$ cross-sections through the respective single-objective focal intensities are shown. To the right of the pupil phase functions, the respective cross-sections through the 4Pi-PSFs are displayed. Here all results are calculated for mode coefficient values of 1 rad (~0.16 λ) rms. Each shown focal intensity is normalized to its own peak intensity.

Optics EXPRESS

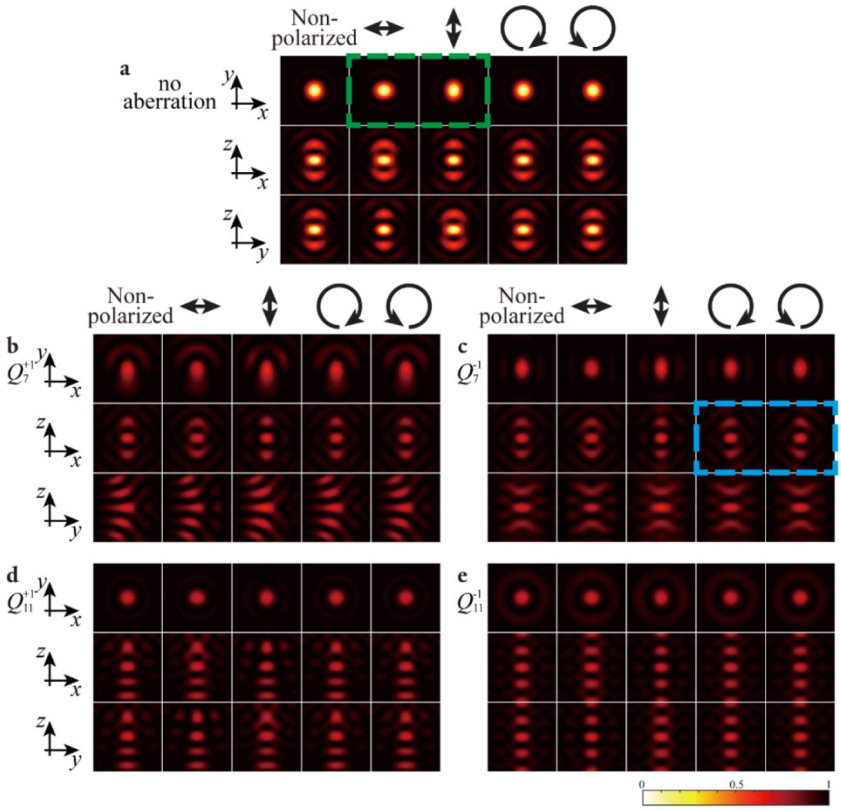

Fig. 5. Influence of polarization on the focal intensity. (a) aberration-free focal intensities. (b) 4Pi coma mode (Q_7^{+1}). (c) 4Pi anti-coma mode (Q_7^{-1}). (d) 4Pi spherical aberration mode (Q_{11}^{+1}). (e) 4Pi anti-spherical aberration mode (Q_{11}^{-1}). In each figure, the $xy|_{z=0}$ (the 1st row), $xz|_{y=0}$ (the 2nd row), and $yz|_{x=0}$ (the 3rd row) cross-sections through the respective 4Pi focal intensities are shown. For each column in the figures, from left to right, the input beams are unpolarized, *x*-linearly polarized, *y*-linearly polarized, clockwise circular polarized, and counter-clockwise circular polarized.

In contrast, the focal intensities induced by contra-variant modes do not have analogs in single-objective systems (Figs. 4(b) and 4(d)). Interestingly, they show a remarkable degree of lateral and axial symmetry. This can be explained by the fact that the superimposed foci stemming from the upper and lower beam path have been distorted in opposite directions: if one beam path suffers a distortion of one orientation, the other path produces the same distortion on the opposite side.

As most 4Pi microscopes are equipped with high-NA objectives, the effects of polarization are complex. For example, the high NA causes mixing of one polarization direction into the other two [19] which has visible impact on the symmetry of 4Pi focal intensities for some contra-variant 4Pi modes. In some 4Pi systems, polarization manipulation has even been applied as an effective strategy for PSF engineering [20]. For these reasons, we further investigated the combined effects of aberrations and polarizations. For different polarizations, a given aberration results in diverse distortion phenomena. We examined the effects of linear and circular polarizations and compared the results with those originating from unpolarized incident beams. In both cases (polarized and unpolarized incident beams), in an aberration-free 4Pi system, the focal intensity is symmetrically distributed with respect to the optical (*z*) axis (Fig. 5(a)). Specifically, when linearly polarized incident beams are

Optics EXPRESS

applied, the focal intensity is slightly stretched in the polarization direction (highlighted by a green rectangle in Fig. 5(a)). The lateral symmetry of focal intensities is preserved when 4Pi aberration modes originating from Zernike polynomials of even azimuthal order (e.g. 4Pi modes with indices 4 to 6 and 11 to 15), are added (Figs. 5(d) and 5(e)). In contrast, 4Pi aberration modes originating from Zernike polynomials of odd azimuthal order (e.g. 4Pi modes with indices 2, 3, and 7 to 10) break this lateral symmetry (Figs. 5(b) and 5(c)). Still taking coma as an example, for both polarized and unpolarized input beams, if *y*-coma Q_7^{+1} is introduced in a 4Pi microscope, the intensity in the focal (*xy*) plane is distorted (Fig. 5(b)), having a side-lobe in the y direction. This asymmetry is dominated by the lateral components ($|\mathbf{E}_x|$ and $|\mathbf{E}_y|$), while $|\mathbf{E}_z|_{z=0} \equiv 0$ (Figs. 6(a) and 6(b)). For the contra-variant coma mode (*y*-anti-coma Q_7^{-1}), the focal intensity is less distorted (but is slightly stretched in the *y* direction) (Figs. 5(c), 6(c), and 6(d)), and the electrical fields of all three polarization components maintain symmetry in the *xy* and *yz* planes with respect to the optical axis. In the plane perpendicular to the stretching direction (*xz* plane), the symmetry is still preserved when the input beams are unpolarized or linearly polarized. However, the symmetry is broken when the input beams are circularly polarized (highlighted by a blue rectangle in Fig. 5(c)), mainly due to the strongly distorted E_z field (Fig. 6(c)). If the polarization handedness is changed (from clockwise to counter-clockwise), the distorted focus induced by the contra-variant mode is inverted about the optical axis (Fig. 6(d)).

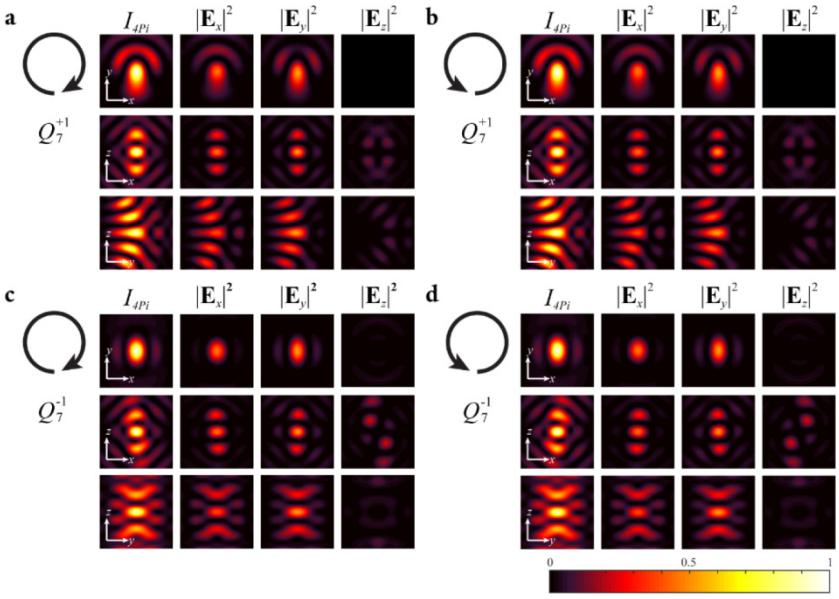

Fig. 6. Influence of circular polarization on the total focal intensity and the focal intensity of each polarization component ($|\mathbf{E}_x|^2$, $|\mathbf{E}_y|^2$ and $|\mathbf{E}_z|^2$) for covariant and contra-variant 4Pi modes of odd azimuthal order (at the example of coma and anti-coma modes). In (a) and (c), the incident beam has clockwise circular polarization, while (b) and (d) show counter-clockwise circular polarization. (a) and (b) 4Pi coma mode. (c) and (d) 4Pi anti-coma mode. All figures are calculated for a mode coefficient value of 1 rad (~0.16 λ) rms. Each figure is normalized to its own peak intensity.

To correct for aberrations in 4Pi microscopes, we can place phase modulators, such as deformable mirrors (DMs), into the upper and lower paths. To directly manipulate the complex pupil function, the DMs are conjugated to the back pupils of both objectives by

Optics EXPRESS

telescopes. These two DMs are conjugated with each other, and the introduced 4Pi modes allow us to control the phase as if there is only one adaptive element in a single control loop. This setup therefore is compatible with both sensorless and sensor-based adaptive optics (AO) methods [21]. In practice, a similar layout has already been integrated into a 4Pi-SMS nanoscope to add astigmatism and to expand the axial imaging range to the whole-cell level [10]. However, in Ref [10], the two DMs were still considered as separate devices. With the aberration model proposed here, we are able to manipulate the phase, and further the PSF, using a single set of coefficients.

A further advantage of the modal representation we have introduced here concerns the different effects of the 4Pi modes in para-illumination configuration (as discussed already, where the sample is illuminated simultaneously from both sides) and transmission configurations (where illumination through one objective passes through the specimen and is collected by the second objective). Such a transmission configuration might be employed in an attempt to perform aberration measurement in an adaptive optical system. These measurements will be insensitive to all covariant modes, as defined here, even though focal distortion would occur. In effect, a system where such a mode is present would introduce an aberration in light passing to the focus that is then removed on the subsequent path from the focus to the second objective. In contrast, a contra-variant mode would lead to a measurement of the underlying Zernike mode, but with double the amplitude. Understanding these different effects are essential in predicting the operation of a trans-illuminated measurement scheme.

4. Summary

In conclusion, we have introduced an orthogonal and complete set of pupil phase functions that describes (monochromatic) aberrations in 4Pi microscopy in a holistic way rather than separated into two beam paths. This set is generated by the combinations of Zernike polynomials from the upper and lower paths in a 4Pi-cavity. Appropriate classification of these modes allows the representation of physical phenomena in particular modes, such as focal displacement or objective positioning error. Such a formulation will aid the simultaneous control of aberrations in two pupils by adaptive optics. By representing aberrations in this manner, the implementation of sensorless image-based AO schemes is made simpler, as one can consider the dual DMs as a single element with a single set of control modes. The new modes may also be useful in AO systems employing wavefront sensors. However, this would depend upon the exact configuration of the system, particularly with respect to the placement of the sensors and the choice of "guide star" (for example, whether it is a point source in the specimen, or a beam transmitted through the specimen). A full discussion of this is beyond the scope of this paper. However, it is important to note that these aberrations are not the only cause for PSF distortions in 4Pi microscopy. Other parameters, including polarization, chromatic aberrations, balance of intensities in the two arms and coherence of light, have additional influence and need to be carefully considered.

Besides aberration compensation, 4Pi modes further allow the expansion of the applications of phase retrieval approaches [22, 23] to 4Pi microscopy which opens the door for more advanced PSF engineering, such as structured illumination for 3D super-resolution imaging, and multiple foci for parallel imaging.

Funding

Wellcome Trust (095927/A/11/Z, 095927/B/11/Z, 203285/B/16/Z, 203285/C/16/Z), the G. Harold & Leila Y. Mathers Foundation, the National Institutes of Health (P30 DK45735) and European Research Council (AdOMiS, no. 695140).

Acknowledgement

J. B. discloses significant financial interest in Bruker Corp. and Hamamatsu Photonics.